

Multi-factor Physical Layer Security Authentication in Short Blocklength Communication

Miroslav Mitev, Mahdi Shekiba-Herfeh, *Member, IEEE*, Arsenia Chorti, *Senior Member, IEEE*, Martin Reed, *Member, IEEE*

Abstract—Lightweight and low latency security mechanisms are becoming increasingly important for a wide range of Internet of things (IoT) applications. Promising schemes from the physical layer include (i) physical unclonable functions (PUFs), (ii) localization based authentication, and, (iii) secret key generation (SKG) from wireless fading coefficients. In this paper, we focus on short blocklengths and propose a complete, fast, multi-factor authentication protocol that uniquely combines PUFs, proximity estimation and SKG. To demonstrate the performance of the SKG scheme in the short blocklength (with a focus on delay constrained applications), we provide a numerical comparison of three families of channel codes, including low density parity check codes (LDPC), Bose Chaudhuri Hocquenghem (BCH), and, Polar codes. The SKG keys are incorporated in a zero-round-trip-time resumption protocol for fast re-authentication. All schemes of the proposed mutual authentication protocol are shown to be secure through formal proofs using Burrows, Abadi and Needham (BAN) and Mao and Boyd (MB) logic as well as the Tamarin-prover.

I. INTRODUCTION

Authentication is central in building secure Internet of things (IoT) networks; confirming the identity of devices and their role in the network hierarchy eliminates the possibility of numerous attacks [1]. However, the low latency and computational power constraints present in many IoT systems [2], render the design of IoT authentication mechanisms a challenging task. Current solutions rely on modulo arithmetic in large fields and typically incur considerable latency, in the order of tens of milliseconds; as an example, it has been reported that verifying digital signatures on a vehicle with a 400 MHz processor takes around 20 msec [3], exceeding the delays that are tolerated in vehicle to everything (V2X) communications. In this direction, a 3GPP report on the security of ultra reliable low latency communication (URLLC) systems notes that authentication for URLLC is still an open problem [4]. On a more general note, with the advance of quantum computing, traditional asymmetric key cryptographic schemes will become semantically insecure, unless the key sizes increase to impractical lengths. Therefore, the introduc-

tion of new security primitives for device authentication is timely.

In this sense, physical layer security (PLS) has proven itself as a lightweight alternative to the computational complexity based mechanisms [5], [6]. The increasing interest in PLS has been stimulated by many practical needs. Notably, many critical IoT networks require fast authentication, e.g., in V2X applications, telemedicine and haptics. Moreover, PLS, that relies upon information-theoretic security proofs, could resist quantum computers, unlike corresponding asymmetric key schemes relying on the (unproven) intractability in polynomial time of certain algebraic problems.

PLS schemes exploit physical layer entropy sources, including both in the hardware, as well as in the communication medium [7]–[9]. With respect to the former, physical unclonable functions (PUFs) are hardware entities harnessing entropy from physically unclonable variations that occur during the production process of silicon [10], [11]. These unique and unpredictable variations allow the extraction of uniformly distributed binary sequences that can be used as authentication IDs or keys. Due to their unclonability and simplicity, PUFs are seen as lightweight security primitives that can offer alternatives to today’s authentication mechanisms.

Moreover, a straightforward secret key generation (SKG) approach can be built by exploiting the reciprocity of the wireless fading coefficients between two terminals within the channel coherence time. When SKG and PUF encoders are employed in URLLC systems, it is critical to employ good error correction codes so as to achieve good reliability without any information leakage, while operating in the short blocklength. The employed codes should be able to reconcile any mismatched bits with high probability (reliability) while on the other hand they should not reveal any information about the key (security).

Following from the above, in this work we introduce a fast, multi-factor authentication protocol for short blocklength communication. To achieve a high security level the proposed scheme combines the following set of factors: 1) PUFs that are used as hardware fingerprints of IoT devices; 2) quick proximity verification using the received signal strength indicator (RSSI); and, 3) SKG to generate symmetric resumption keys used to speed up authentication by resuming sessions (as opposed to re-establishing sessions). With respect to SKG, we further provide a numerical comparison between different reconciliation encoders in the short blocklength regime, benchmarked against the theoretical upper bound. The aforementioned factors are combined in a PLS resumption protocol

M. Mitev, M. Shakiba-Herfeh and A. Chorti are with ETIS UMR8051, CY Cergy Paris University, ENSEA, CNRS, F-95000, Cergy, France ({miroslav.mitev, mahdi.shakiba-herfeh, arsenia.chorti}@ensea.fr);

M. Reed is with the CSEE, University of Essex, Colchester (mjreed@essex.ac.uk), UK;

M. Mitev is supported by the DIM RFSI project SAFEST; M. Shakiba-Herfeh and A. Chorti are supported by the ELIOT ANR-18-CE40-0030 - FAPESP 2018/12579-7 and the INEX Project eNiGMA; M. Reed is supported by the H2020 project SerIoT with project agreement no 780139 funded by the EU.

that allows for data exchange within zero-round-trip time (0-RTT). Finally, the security of the authentication protocol is verified through formal methods: Burrows, Abadi, Needham (BAN) [12] as well as Mao and Boyd (MB) logic and the Tamarin-prover [13].

The main contributions of this paper are as follows:

- 1) We discuss the performance of three families of codes in the short blocklength for Slepian Wolf (SW) based SKG reconciliation.
- 2) We propose a lightweight and fast proximity detection using Kalman filters, suitable for constrained IoT devices.
- 3) We introduce a forward secure 0-RTT resumption authentication mechanism.
- 4) We develop a fast multi-factor authentication protocol that combines an initial proximity check with PUF authentication and SKG resumption keys.
- 5) We formally prove the security of the proposed individual schemes and of the full protocol.

The rest of the paper is organized as follows: Section II discusses related work, Section III discusses the performance of different short blocklength SKG reconciliation encoders. Section IV introduces a fast proximity estimation mechanism and Section V presents the proposed authentication protocol whose security properties are verified in Section VI. Finally Section VII concludes this paper.

II. RELATED WORK AND CONTRIBUTIONS

It is well established that SKG can be performed at PHY by using the channel fading as a source of common randomness. During the channel's coherence time, two parties, referred to as Alice and Bob in the following, can observe highly correlated channel states that can be used to generate a shared secret key between them [14]. As Alice's and Bob's measurements differ due to noise, to generate a common key, Slepian Wolf (SW) decoding of the observed sequence is required for reconciliation [15]–[18]. However, most prior works have not considered SW decoding with short blocklengths. In the present work, we implement and compare the performance of three families of SW decoders that show promising performance in short blocklength communication [19], [20].

Furthermore, we introduce a lightweight method of proximity verification, to be employed as an early authentication step. The literature of localization and RF-fingerprinting based authentication is vast, e.g., see the surveys [21], [22]. Although any of the many existing algorithms could be employed in our proposed protocol, here we present an alternative approach in which a (single) mobile unit (typically an IoT node) can verify the proximity of a fixed location node (typically an access point acting as an edge server). To render the scheme robust against impersonation type of attacks, in which a malicious server changes its transmission power to falsify its location information, we leverage mobility. Instead of relying on a single RSSI measurement, we propose taking multiple RSSI measurements that, thanks to their mobility of the authenticating entity, are unpredictable by an attacker. To the best of our knowledge, this approach has only been reported once in the literature so far in the recent paper [23], where the

authors leverage the mobility of a mobile handset to localize a base station using unscented Kalman filters with the time of arrival (ToA) and angle of arrival (AoA) information as inputs. Our proposed proximity estimator is much simpler and faster as it relies solely on RSSI measurements and uses a simple Kalman filter with scalar inputs, so it is an attractive approach for inverse proximity estimation in IoT networks.

Finally, central to our proposed authentication protocol is the role of PUFs. A PUF can be used in a challenge – response authentication protocol, where a challenge can refer to measuring the jitter of a ring oscillator, power-on state, etc. A typical PUF-based authentication protocol consists of two main phases, referred to as *enrollment* and *authentication*, respectively [24]–[26]. During the *enrollment* phase each node runs a set of challenges on its PUF and characterizes the variance of the measurement noise in order to generate helper data. Next, a verifier creates a database with all challenge-response pairs (CRPs) corresponding to the nodes within its network. Later, during the *authentication* phase the verifier sends a random challenge to the corresponding node. The node computes the response by running the challenge on its PUF and sends it to the verifier to confirm its authenticity. Numerous authentication protocols have been proposed based on this approach [27]. However, relying on PUFs as a single security factor can expose the system to a variety of threats, especially in an IoT scenario [28]. In this sense, combining two or more independent credentials can be used to build a secure multi-factor authentication protocol. For example, PUFs have been combined with shared-key [29], localization [24], and channel characteristics [7].

Any two PUF measurements at the same node are never exactly the same due to measurement noise, thus reconciliation between successive measurements is needed. To this end, the verifier uses helper data stored during the enrollment to regenerate the initially derived authentication key. Reconciliation can be implemented using fuzzy extractors (FE) [30]. A FE is built from a pair of randomized functions, i.e., Gen and Rep , where Gen takes as input a PUF response and produces two outputs: helper data and a uniformly distributed key; Rep , which stands for deterministic reproduction, reproduces the key by using the initial helper data and a new noisy version of the response [31]. Overall, authentication is achieved by comparing a key generated from the initial response, to a key generated from a later response. Generally, the Rep function has greater computational complexity than the Gen . In IoT networks it is desirable that the more complex operations are performed on a resourceful device (e.g., an edge server) rather than on a constrained IoT node.

PUF authentication can greatly reduce computational overhead. However, the size of the CRP space of a single PUF is limited. To overcome this limitation, we propose a solution inspired by the 0-RTT authentication mode introduced in TLS 1.3. The 0-RTT feature allows users to send data on the first flight without re-authentication (early data), nevertheless, this fast resumption introduces new vulnerabilities [32]. To address these issues, a secure, mutual authentication protocol is presented. The scheme is multi-factor, i.e., node authentication is verified by: i) the combination of an initial proximity detection

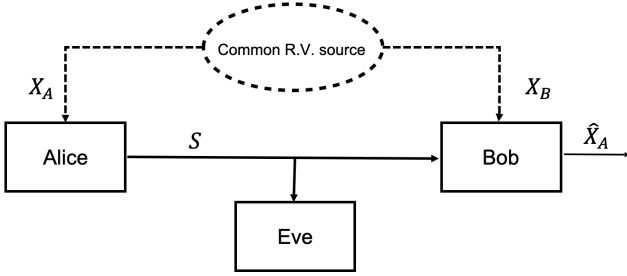


Fig. 1: The system model for coding on secret key generation.

with PUFs and unique session IDs that ensure properties such as untraceability, anonymity, protection against impersonation attacks and many more; and, ii) an additional SKG mechanism that allows for uniform session key generation. By introducing SKG resumption keys in a 0-RTT type of protocol we achieve both forward secrecy and protection against replay attacks.

III. SKG SW DECODING IN THE SHORT BLOCKLENGTH

In this section we focus on SW coding aspects in short blocklengths and implement three different families of codes and compare their performance against a known upper bound. In our system model, we assume Alice and Bob generate binary sequences Y_A, Y_B of length n by quantizing their respective observations of the channel coefficient H_0 , denoted by X_A and X_B , respectively. For simplicity, in this work we assume that a passive adversary, referred to as Eve, cannot obtain any information for the generated sequences¹.

We assume that the generated binary sequences are independent and identically distributed (i.i.d.) with equal probabilities to be 0 or 1, i.e., $Pr(Y_A[i] = 0) = Pr(Y_B[i] = 0) = 0.5, i = 1, \dots, n$. Alice and Bob aim to agree on a secret key K of length k that needs to be drawn uniformly from $K = \{0, 1\}^k$. To this end, Alice transmits her syndrome S_A , of length $n-k$, through a public channel to assist Bob to obtain an estimate \hat{Y}_A of her sequence Y_A . The code rate is defined as $R = \frac{k}{n}$ and the frame error rate (FER) is defined as the probability that Bob's estimation of Y_A is erroneous $Pr(Y_A \neq \hat{Y}_A)$. In this set-up, Bob first estimates the sequence \hat{Y}_A and then based on that, Alice and Bob independently extract the key K using privacy amplification (Fig. 1).

Motivated by the promising performance of low density parity check codes (LDPC) [36], polar codes [37] and Bose Chaudhuri Hocquenghem (BCH) codes [38] with list decoding in short blocklengths for standard channel coding applications, in this paper we implement and compare against the upper bound in [39] the SKG achievable rates when these three families of SW decoders are employed.

A. LDPC codes with ordered statistic decoding

LDPC codes are powerful error correcting codes that can approach the Shannon limit [40] at very large blocklengths.

¹Due to large scale fading and path-loss, the channel coefficients between Alice, Bob and Eve are typically correlated. However, it is possible through pre-processing of the coefficients to remove correlations with the observation of Eve, e.g., see [33], [34], [35]. In the rest of this paper, for compactness of presentation we assume this assumption holds.

However, in general, LDPC codes do not perform well in short blocklengths. To address such shortcomings, LDPC codes enhanced with ordered statistic decoding (OSD) is one of the techniques that has been suggested to achieve near maximum likelihood (ML) performance for short blocklengths [36]. The central idea behind OSD is that first we pick the \tilde{k} most reliable independent positions, where \tilde{k} is the rank of the code. Then, based on the log-likelihood ratios (LLR) we make hard decisions on the value of the selected bits. Subsequently, we generate a candidate list of codewords by flipping the values of up to t bits among them. Finally, by performing ML search in the list we choose the most likely codeword [41]. The size of the candidate OSD list increases with respect to t as $\sum_{i=0}^t \binom{k}{i}$. In our implementation, Bob first feeds Y_B and S_A to the LDPC decoder to generate soft information of the bits (i.e., the LLRs). Then the LLRs are passed to the OSD block to estimate \hat{Y}_A . The public message is given as $S_A = Y_A H^t$, where H^t is the transpose of the parity check matrix.

B. Polar codes with list decoding

Polar codes are linear block error correcting codes that can provably achieve the capacity of a binary-input discrete memoryless channel as the code length tends to infinity [42]. A significant improvement in the performance of polar codes in finite blocklengths can be achieved by utilizing successive cancellation list decoding, that keeps a list of most likely decoding paths. List decoding can be improved further by utilizing cyclic redundancy check (CRC). The CRC assists the decoder to pick the correct decoding path in the list, even if it is not the most probable one [37].

In our implementation (similar to [43]), Alice encodes her sequence Y_A as $U = Y_A G_n$, where $G_n = \begin{pmatrix} 1 & 0 \\ 0 & 1 \end{pmatrix}^{\otimes n}$ is the encoder matrix as defined in [43]. Alice sends the syndrome S_A which contains S_1 and CRC bits with length l . S_1 has length $n-k-l$ and contains high-entropy bits of U as follows

$$H(U[i]|Y_A, U^{i-1}) \geq H(U[j]|Y_A, U^{j-1}), 1 \leq i, j \leq n, \quad (1)$$

where i is the position of transmitted bits and $H(\cdot)$ denotes entropy. Therefore, the actual rate of the polar code is $R = \frac{k+l}{n}$. On the other side, Bob applies CRC-aided successive cancellation list decoding to estimate \hat{Y}_A . Note that the complexity of list decoding polar coding grows linearly with the list size.

C. BCH codes with list decoding

BCH codes are a class of cyclic error-correcting codes constructed by polynomials over a finite field. One of the main features of BCH codes during code design is the number of guaranteed correctable error bits. A binary BCH code is defined by $(n_{BCH}, k_{BCH}, t_{BCH})$, where $n_{BCH} = 2^w - 1$ is the blocklength, k_{BCH} is the message length, and t_{BCH} represents the number of guaranteed correctable error bits. To improve their error correcting capability, BCH codes can be armed with list decoding.

In our implementation of list decoding, Alice calculates the syndromes as $S_A = Y_A H^t$, where H is the parity check matrix of the BCH code, and transmits it through the public channel.

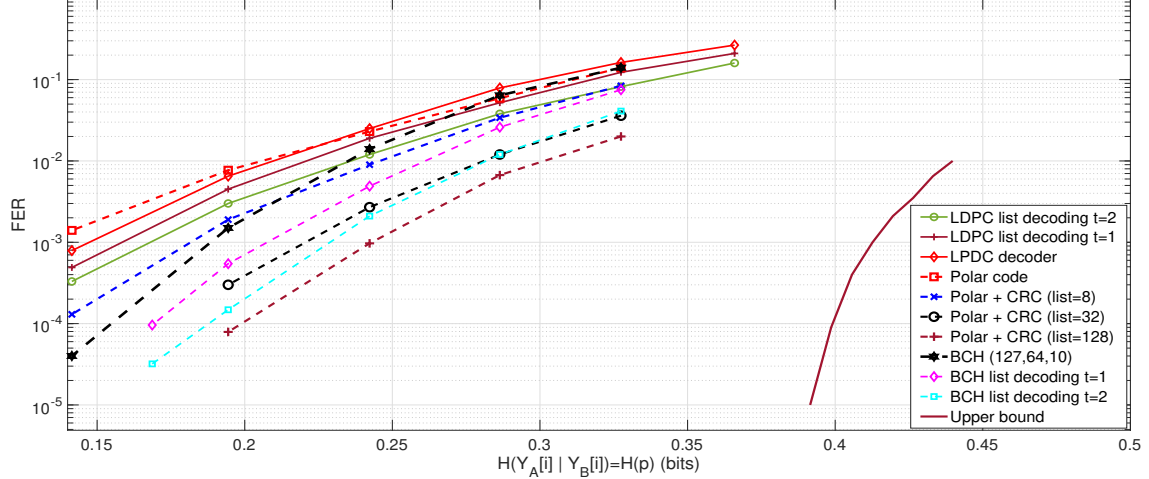


Fig. 2: Comparison of FER performance of codes with the upper bound in [39] for $n = 128$.

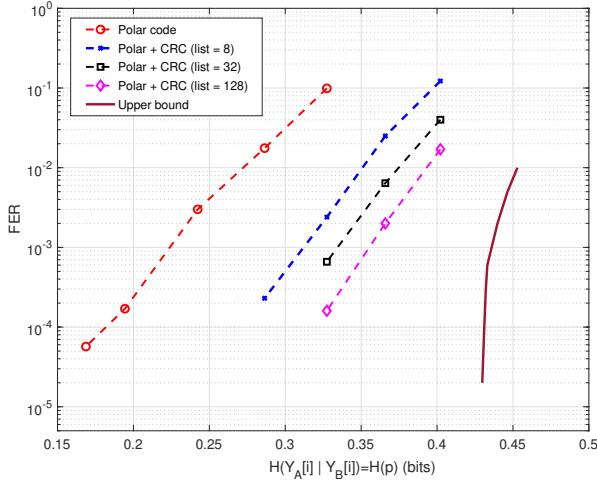


Fig. 3: Comparison of FER performance of polar code with the upper bound in [39] for $n = 1024$.

On the other side, Bob, first generates a candidate codeword list by flipping up to t bits of the measured sequence Y_B . After feeding the list to the BCH decoder, it picks the solution which has the lowest Hamming distance with the measured sequence Y_B . In our implementation of list decoding, the size of the list increases with respect to t as $\sum_{i=0}^t \binom{n}{i}$.

D. Numerical results

In this subsection, we analyse the FER performance of the aforementioned codes in the SKG setting and compare them with the finite length upper bound reported in [39], noting that optimization of the degree distributions is out of the scope of this study. For instance, we consider $n = 128$ and we implement a $(n, k) = (128, 75)$ polar code with 11 bits CRC and a $(127, 64, 10)$ BCH code. Also, we pick regular

$(3, 6)$ LDPC codes with length 128 bits². In Fig. 2, the FER performances of half rate codes with 128 bits blocklength are depicted (i.e., the key length after privacy amplification is 64) and compared to the upper bound reported in [39]. Note that the upper bound becomes inaccurate for short blocklength while their accuracy improves as the blocklength increases. That is the reason we observe comparatively a large gap between the upper bound and the codes' FER performances for $n = 128$ [18].

As it is depicted in Fig. 2, the polar code with list size 128, and the order two BCH list decoding code show the best performance among the codes. Also, the results demonstrate that although classical polar codes do not perform well in the short blocklength, their performance can be significantly improved by arming them with list decoding. For example, the polar code with list size 128, provides around two orders lower FER compared to the classical polar code at $H(Y_A[i] | Y_B[i]) = 0.1944$. However, this improvement comes at the cost of 128 times more decoding complexity. List decoding also improves the performance of the BCH code, but the improvement with respect to the additional complexity is not as notable as in the case of the polar code. The improvement in the LDPC code performance is still observed by using OSD, however it is not very significant.

Moreover, we consider an instance of $n = 1024$. In Fig. 3, the FER performances of a half rate polar code with $(n, k) = (1024, 523)$ and 11 bits CRC for different list sizes are shown. As it is demonstrated in Fig. 3, utilizing list decoding can significantly improve performance. For a list size larger than 8, the improvement by increasing the size of the list is not significant. Also we observe that, at blocklength $n = 1024$, the gap between the FER of the polar code and the upper bound is less than the case $n = 128$. We posit that one of the reasons is that the upper bound at this length is tighter than the first instance.

²We note that the performance of LDPC codes can be improved by optimizing the variable and check nodes degree distributions [44], however the degree optimization of the LDPC codes is out of the scope of this work.

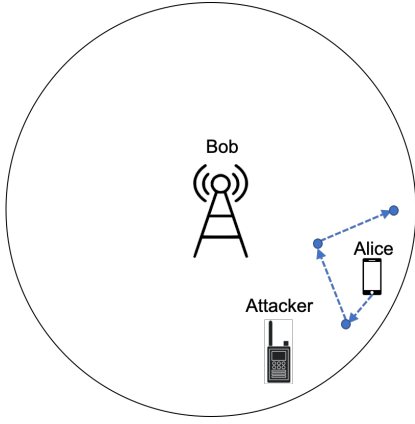


Fig. 4: Proposed proximity estimation.

IV. FAST PROXIMITY ESTIMATION

Introducing a “smart movement” environment brings number of advantages to IoT systems, including energy saving, control over the node mobility and increased overall quality-of-experience (QoE) [45]. In this direction, we propose in this Section a fast proximity estimation approach, based on the mobility of IoT devices. The novelty in our strategy relies upon the fact that if Alice (a mobile IoT node) moves in a manner unpredictable for adversaries, she can take successive measurements of the RSSI and use them for proximity estimation of a static Bob (e.g., a static edge server), as shown in Fig. 4. In fact, this lightweight proximity estimation approach allows Alice to detect impersonation attacks³ when used in combination with the authentication protocol presented in the next section.

Due to the ease of implementation and signal availability, RSS-based localization is usually a favoured technique. According to the inverse-square law, the RSSI at Alice can be used to estimate the distance between her and Bob. We assume that the channel coefficients follow a log-normal power distribution. In this sense, the traditional path loss model for noisy environment is [46], [47]:

$$P(dBm) = P_0(dBm) - 10n \log_{10} \left(\frac{d}{d_0} \right) + X_\sigma, \quad (2)$$

where P is the strength of the received signal in dB, P_0 represents the average received signal strength at some reference distance d_0 in dB, d is the distance of the transmitter, n is an attenuation factor that gives the relation between distance and received power, and $X_\sigma \sim \mathcal{N}(0, \sigma_{X_\sigma}^2)$ is a zero mean Gaussian random variable modelling shadowing [48]. Based on the model for noisy RSSI, the distance can be estimated as [49]:

$$\hat{d} = d_{10} \frac{P_0 - P}{10n} e^{-\frac{1}{2} \left(\frac{\sigma_{X_\sigma} \ln(10)}{10n} \right)^2}. \quad (3)$$

Finally, we employ a Kalman filter for the proposed proximity algorithm. A Kalman filter can successfully lower the impact

³An impersonation attack when proximity estimation is used as an authentication factor can be mounted by altering the transmission power level, e.g., as in some false base station types of attack. By taking successive measurements of the RSSI in unpredictable locations, this attack can be mitigated.

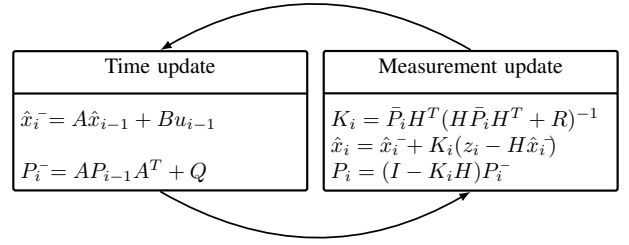


Fig. 5: Kalman filter steps

of noise present in the RSSI and thus improves the reliability of the proposed localization approach. The filter’s parameters are usually in the form of matrices, however, the target in the scenario assumed here is static, and as a result all parameters reduce to scalar values. This greatly reduces the complexity of the filter and makes the algorithm suitable for a resource constrained device (for details on Kalman filters see [50]). The filter works by the assumption that the current state x_i has a relation to the previous state x_{i-1} , and this relation is expressed as follows:

$$x_i = Ax_{i-1} + Bu_{i-1} + w_{i-1}, \quad (4)$$

where the transition matrix A links the current state x_i with the previous one x_{i-1} , B is a control matrix which relates the control vector u to the state and w is i.i.d. normally distributed process noise such that $w \sim \mathcal{N}(0, Q)$. Following that a measurement is given by $z_i = Hx_i + R_i$, where H is an observation matrix used to translate each state to a measurement and R is i.i.d. normally distributed measurement noise such that $R \sim \mathcal{N}(0, \sigma_R^2)$.

Given the above, the recursive process of the filter is presented in Fig. 5. It is based on two main steps: prediction and correction (time and measurement update, respectively). During the time update step: i) the next state is updated based on the previous state; ii) the error covariance matrix P is updated. In the above \hat{x}_i^- and P_i^- are the *a priori* estimated state and covariance matrix, respectively. Next, during the measurement update step: i) the so called Kalman gain K is computed; ii) the estimate is updated based on the measurement using the Kalman gain; and, iii) the error covariance matrix is updated using the Kalman gain. In the following subsection, we provide the details of our implementation of the fast proximity estimation using a simple Kalman filter.

A. Implementation of the fast proximity algorithm

We have performed a set of experiments at two different environments: i) in a small auditorium; and, ii) in a library. In both scenarios we had a static Bluetooth low energy (BLE) beacon, transmitting at 1 dBm and a smartphone (mobile node) measuring the RSSI at different locations. This decision is motivated by the scenario assumed for this study, i.e., the access point (Bob) is fixed while the mobile IoT device (Alice) takes consecutive proximity measurements. The line of sight between the two devices was not always present due to moving people in the area. Moreover, there were other BLE and WiFi devices in the vicinity, causing further interference.

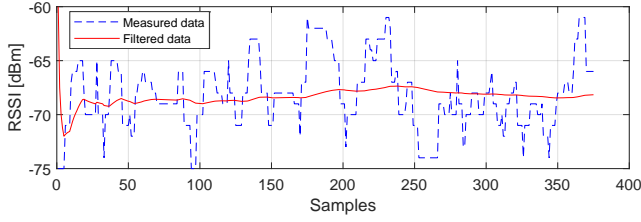


Fig. 6: Measured RSSI data (dashed) and filtered data using Kalman filter (solid) at distance of 3 meters. The measurement noise variance is set to $\sigma_R = 0.1$.

TABLE I: Estimation of channel parameters for both scenarios

Scenario	P_0	n	σ_{X_σ}
Small auditorium	-60.12 @ 1m	1.7	6.49
Library	-61.91 @ 1m	1.85	6.30

First, in Fig. 6, we demonstrate the performance of the Kalman filter. The chosen parameters are as follows: the prediction of the error variance was set to $P_{e,i-1} = 0.1$; the process variance to $Q = 10^{-6}$; the measurement noise variance for the specific environment was chosen as $\sigma_R = 0.1$. The figure shows that the filtered data quickly stabilizes eliminating the noise in the measurements, while the raw RSSI data wildly fluctuated by tens of dBms.

Next, the path loss model for each environment was determined. In both scenarios the smartphone was used to measure the RSSI at different distances from the BLE beacon (1, 3, 6 meters). For each distance, we performed 50 measurements while during each measurement the mobile device collected 20 samples of the RSSI. The motivation behind this value is that in a realistic online phase, Alice could quickly (in a matter of seconds) collect 20 samples. Furthermore, as it can be seen in Fig. 6 even before the 20th sample the Kalman filter has already converged and its output varies only by a few dBms. Therefore, for our proximity estimation we assume that the 20th output of the Kalman filter is the “decision” output which Alice uses to determine her distance to Bob.

The curve fitting of the path loss model in both scenarios is given in Fig. 7. The curves show the standard deviation of the collected RSSI data and the standard deviation of the “decision” outputs of the Kalman filter. The estimated channel parameters for both scenarios are given in Table I. Finally, the distance estimations based on (3) using the collected RSSI data and the “decision” outputs of the Kalman filter are shown in Fig. 8. Overall, in Figs. 7 and 8 it can be seen that the Kalman filter greatly improves the reliability of the proposed method. As expected, the signal strength decreases as the distance increases. Furthermore, it can be observed that the environmental impact over the signal, such as noise and objects, increases at greater distance. This directly influences the distribution of the RSSI and increases the variation from the mean value. However, at the output of the Kalman filter these variations are limited and the mobile node (Alice) can successfully determine whether the static access point (Bob) is in one of the three regions: immediate (1 m), near (3 m), or far (6 m). Moreover, since Alice moves in

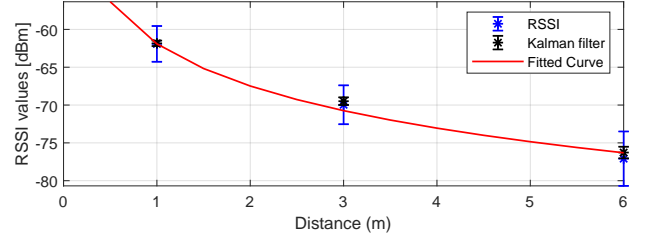
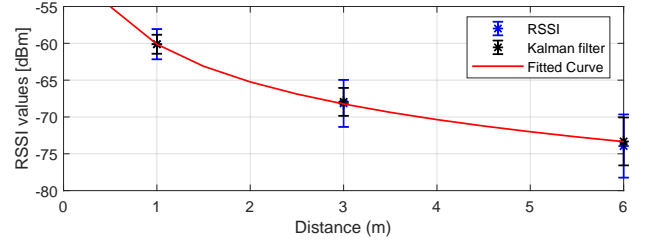


Fig. 7: Curve fitting of the path loss model for a small auditorium (TOP) and a library (BOTTOM).

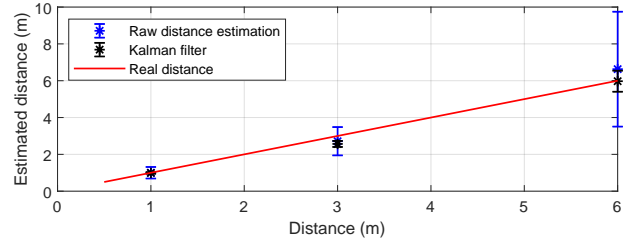
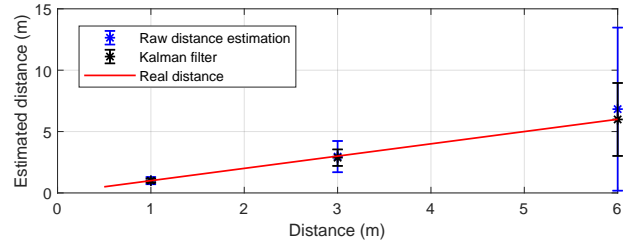


Fig. 8: Distance estimation for a small auditorium (TOP) and a library (BOTTOM).

a manner that is unpredictable for adversaries, a malicious node cannot impersonate Bob unless they are co-located. This simple proximity estimation technique is used as an independent factor in a multi-factor authentication protocol presented in the next section.

V. PROPOSED MUTLI-FACTOR AUTHENTICATION PROTOCOL

This section presents a lightweight multi-factor authentication scheme, leveraging PUFs, proximity estimation and SKG; it consists of two phases: an enrollment phase and an authentication phase and uses SKG as a quick resumption mechanism. We note that in the proposed protocol, only Alice (an IoT node) performs proximity verification. To do so, during the pilot exchange, she positions herself in diverse (unpredictable) locations and takes multiple measurements of the RSSI. The RSSI is used to estimate Bob’s location as discussed Section IV.

We first present all individual primitives and then provide an overall security analysis. The notation used throughout this section is defined as follows:

- A SKG scheme generating as outputs binary vectors K and S_A of sizes $k = |K|$ and $|S_A|$, respectively, with $K \in \mathcal{K}$ denoting the key obtained after privacy amplification and $S_A \in \mathcal{S}$ denoting Alice's syndrome.
- Alice's PUF denoted by P_A that generates a response $R \in \mathcal{R}$ to a challenge $Ch \in \mathcal{Ch}$, i.e., $R = P_A(Ch)$. Also, a pair of fuzzy extractor algorithms, denoted by $\text{Gen} : \mathcal{R} \rightarrow \mathcal{K}_R \times \mathcal{H}_R$, accepting as input the PUF response and generating as outputs the identification (fuzzy) key and helper data, with corresponding reproduce algorithm $\text{Rep} : \mathcal{R} \times \mathcal{H}_R \rightarrow \mathcal{K}_R$, such that:

$$\text{Gen}(R) = (H_R, K_R), \quad (5)$$

$$\text{Rep}(R', H_R) = K_R, \quad (6)$$

where $R, R' \in \mathcal{R}, K_R \in \mathcal{K}_R$ and $H_R \in \mathcal{H}_R$.

- A symmetric encryption algorithm, e.g., AES-256 in Galois field counter mode (GCM)⁴, denoted by $\text{Es} : \mathcal{K} \times \mathcal{M} \rightarrow \mathcal{C}_T$ where \mathcal{C}_T denotes the ciphertext space with corresponding decryption $\text{Ds} : \mathcal{K} \times \mathcal{C}_T \rightarrow \mathcal{M}$, i.e.,

$$\text{Es}(K, M) = C,$$

$$\text{Ds}(K, C) = M,$$

for $M \in \mathcal{M}, C \in \mathcal{C}_T$.

- A pair of message authentication code (MAC) algorithms, denoted by $\text{Sign} : \mathcal{K} \times \mathcal{M} \rightarrow \mathcal{T}$, with a corresponding verification algorithm $\text{Ver} : \mathcal{K} \times \mathcal{M} \times \mathcal{T} \rightarrow \{yes, no\}$:

$$\text{Sign}(K, M) = T,$$

$$\text{Ver}(K, M, T) = \begin{cases} yes, & \text{if integrity verified} \\ no, & \text{if integrity not verified} \end{cases}$$

- A cryptographic (irreversible) one-way hash function

$$\text{Hash} : \{0, 1\}^q \rightarrow \{0, 1\}^k,$$

that is used to compress the size of an input binary vector of length q to a binary vector of length $k = |K|$.

In all of the previously defined functions, the insertion of an index $i - 1$ denotes the value of a variable or quantity one instance earlier than its corresponding value at instance i , e.g., Ch_1 denotes the PUF challenge at instance 1 while Ch_2 denotes the PUF challenge at instance 2. Furthermore, following from the definition of PUFs, every challenge produces a unique response and corresponding helper data and authentication keys, i.e., $P_A(Ch_1) \neq P_A(Ch_2)$ and $\text{Gen}(P_A(Ch_1)) \neq \text{Gen}(P_A(Ch_2))$. Finally, concatenation of two binary vectors X and Y is denoted by $(X||Y)$.

A. Device enrollment

The enrollment is a one-time operation carried out over a secure channel between Alice (referred to in the following as node A) and Bob (referred to in the following as node B).

⁴We note that using a block cipher such as AES-256 in a GCM operation allows to the use of the same key K to encrypt typically Gigabytes of data.

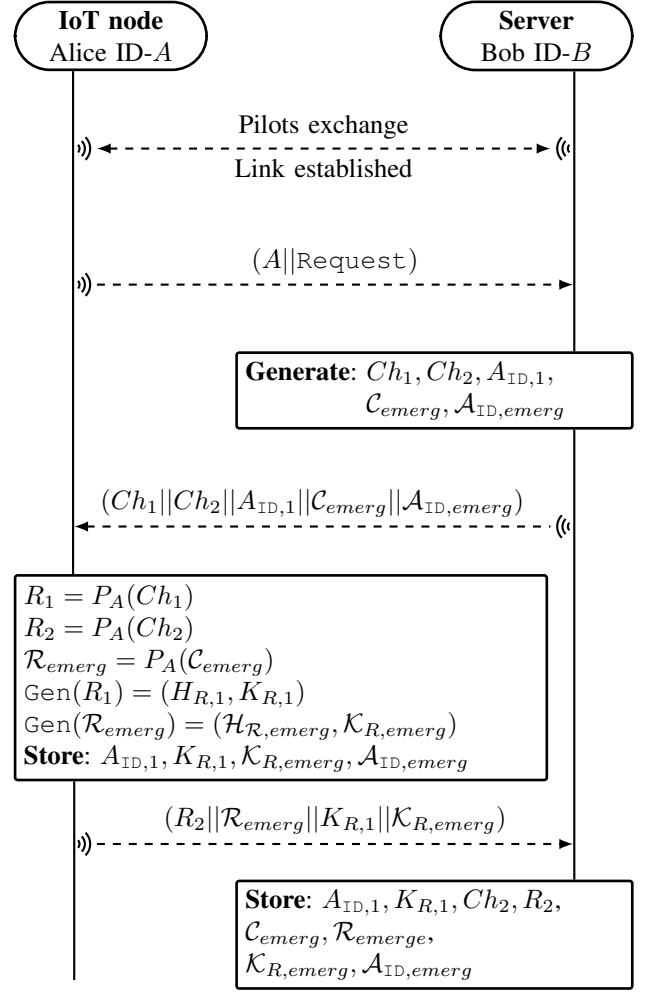


Fig. 9: Enrollment phase

The steps taken during enrollment are summarized in Fig. 9 and are performed as follows:

- 1) In order to establish the link between them, both devices need to exchange pilot signals. During this exchange A measures the RSSI. Furthermore A downloads (or creates) a map of the premises which contains the location of B to enable proximity based authentication.
- 2) After establishing the connection, Alice sends her ID A with a request for registration Request .
- 3) Upon receiving the request, B first checks if the received ID has already been registered. If B finds the ID within his database the request is rejected. If A has not been registered B generates two initial PUF challenges Ch_1, Ch_2 and an initial one-time alias ID $A_{ID,1}$. These challenges will be used during subsequent authentication and will be updated with each run of the protocol. Next, B generates sets of emergency challenges and one-time alias IDs C_{emerg} and $A_{ID,emerg}$, respectively, such that $|C_{emerg}| = |A_{ID,emerg}|$. The emergency sets are used only in a case of de-synchronisation between the devices and have multiple entries to allow for multiple recoveries. Finally, Bob sends the message $(Ch_1||Ch_2||A_{ID,1}||C_{emerg}||A_{ID,emerg})$ to Alice. Note

that the two emergency sets are linked such that each element has a corresponding one in the other set.

- 4) After receiving the message, Alice excites her PUF P_A with Ch_1, Ch_2 and all challenges from the set \mathcal{C}_{emerg} , producing responses R_1, R_2 and \mathcal{R}_{emerg} , respectively. Next, she uses R_1 and \mathcal{R}_{emerg} as inputs to her fuzzy extractor to generate the pair $(H_{R,1}, K_{R,1})$ and the sets of pairs $(\mathcal{H}_{R,emerg}, \mathcal{K}_{R,emerg})$. Afterwards, Alice stores $A_{ID,1}, K_{R,1}, \mathcal{K}_{R,emerg}, \mathcal{A}_{ID,emerg}$ and sends the following message to Bob $(R_2 || \mathcal{R}_{emerg} || K_{R,1} || \mathcal{K}_{R,emerg})$.
- 5) To finalise the registration process, B stores the following elements that correspond to ID A in his database: initial authentication parameters $A_{ID,1}, K_{R,1}, Ch_2, R_2$ and emergency authentication parameters in case of desynchronisation $\mathcal{C}_{emerg}, \mathcal{R}_{emerg}, \mathcal{K}_{R,emerg}, \mathcal{A}_{ID,emerg}$.

B. Authentication

Once the enrollment is finished, both devices can use the established parameters for authentication. The steps taken during authentication are summarized in Fig. 10 and are performed as follows:

- 1) The devices exchange pilot signals and observe X_A, X_B , respectively, which they subsequently quantize to bit strings Y_A and Y_B , correspondingly. From this step, A also measures the RSSI of the received signals.
- 2) Next, A runs the proximity verification discussed in Section IV to confirm the location of B . If the verification fails, she stops the authentication process. If it succeeds, she completes the steps of the SKG process, calculating her syndrome S_A and key K . The key will be used later as a session key if the authentication is successful. Then, A sends her request for authentication which contains a one-time alias ID $A_{ID,i}$ and a fresh random nonce N_1 .
- 3) Upon reception, B accesses the database and loads the parameters that corresponds to the ID, i.e., CRP (Ch_2, R_2) and key $K_{R,1}$. Then he generates a fresh random nonce N_B and breaks K_{R1} into two parts as follows: $K_{R,1} = (K_{R1,1}, K_{R1,2})$. He uses the first part to encrypt $C_B = \text{Es}(K_{R1,1}, (A || B || Ch_2 || N_1 || N_B))$, and uses the second part to sign M_B as: $T_B = \text{Sign}(K_{R1,2}, C_B)$. Finally, he sends the ciphertext M_B and the signature T_B to A .
- 4) By using her stored key $K_{R,1}$, A verifies the authenticity of B and the integrity of the message M_B . If one of the verification checks fail A rejects the message's claim to authenticity. If the verification succeeds she accepts and excites her PUF with the received challenge Ch_2 . By running it on her PUF she obtains a new measurement $R'_2 = P_A(Ch_2)$ and $\text{Gen}(R'_2) = (H_{R',2}, K_{R',2})$. Afterwards, she generates a new fresh random nonce N_A and calculates the next two challenges as follows: $Ch_3 = \text{Hash}(Ch_2 || N_A)$ and $Ch_4 = \text{Hash}(Ch_3 || N_B)$. Next, she excites her PUF to produce R_3 and R_4 . In order to generate the key that will be used in a future execution of the authentication protocol, A executes $\text{Gen}(R_3) = (H_{R,3}, K_{R,3})$. Next, she calculates the one-time alias ID for future execution of the protocol as

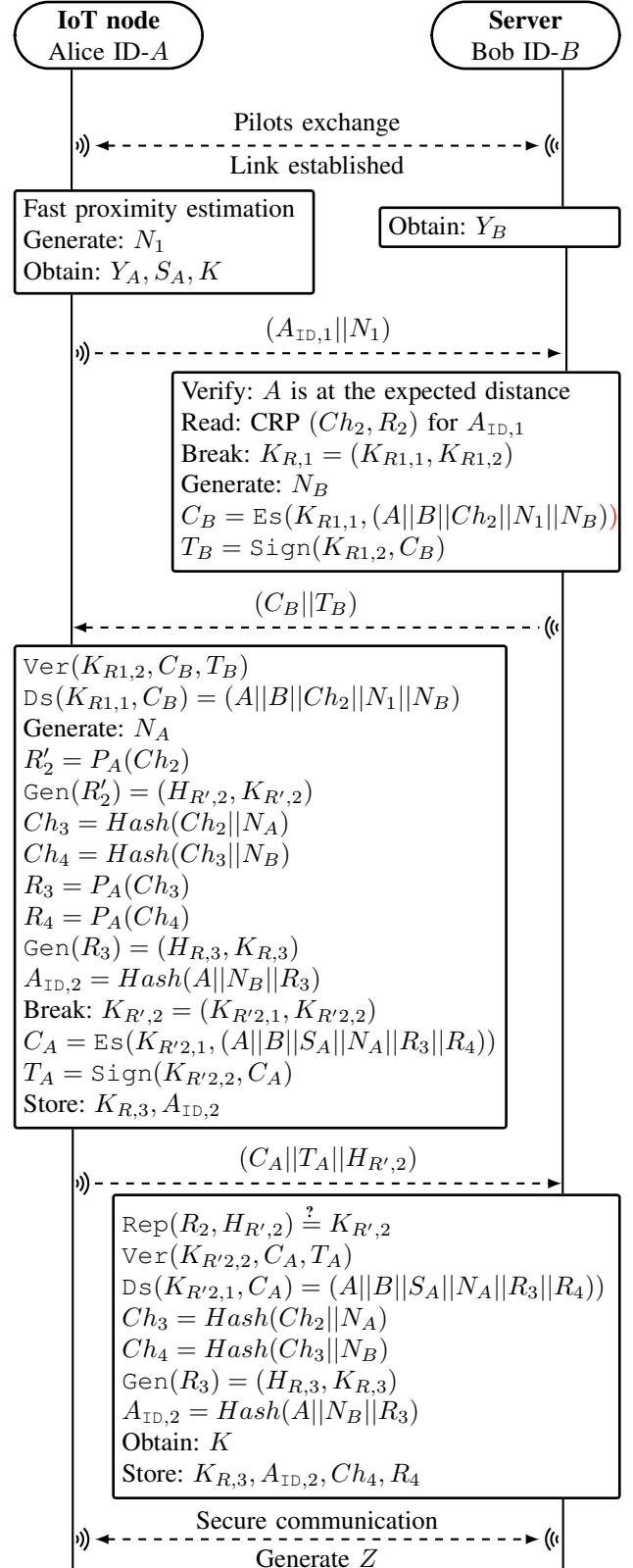


Fig. 10: Authentication protocol

$A_{ID,2} = \text{Hash}(A || N_B || R_3)$ which due to the randomness of N_B and R_3 , cannot be linked to $A_{ID,1}$. The pairs (Ch_4, R_4) and $(K_{R,3}, A_{ID,2})$ will be used in a subsequent connection with B . Next, A breaks her key $K_{R',2}$ into

two parts $K_{R',2} = (K_{R',2,1}, K_{R',2,2})$. Similarly, to the previous step she uses half of the key to encrypt the message $C_A = \text{Es}(K_{R',2,1}, (A||B||S_A||N_A||R_3||R_4))$. Then, A uses the second half of the key to sign the ciphertext $T_A = \text{Sign}(K_{R',2,2}, C_A)$. Finally, A sends C_A, T_A and $H_{R',2}$ to B and stores the pair $K_{R,3}, A_{\text{ID},2}$.

- 5) Upon receiving the preceding message, B verifies the condition $\text{Rep}(R_2, H_{R',2}) \stackrel{?}{=} K_{R',2}$ by using the stored R_2 (from the enrollment phase) and the received helper data $H_{R',2}$. If the verification fails, B rejects the claim to authenticity. If the claim is accepted, he verifies the integrity of C_A using the signed ciphertext T_A . Next, using R_3 and the principles of the fuzzy extractor B performs $\text{Gen}(R_3) = (H_{R,3}, K_{R,3})$. He calculates $A_{\text{ID},2} = \text{Hash}(A||N_B||R_3)$. Following that, he stores the pairs $(K_{R,3}, A_{\text{ID},2}), (Ch_4, R_4)$ which will be used during the next round of the protocol. Finally, using the received syndrome S_A , B corrects the discrepancies in his observation Y_B to obtain Y_A and calculates the session key $K = \text{Hash}(Y_A)$.
- 6) After the authentication process finishes A and B enter the secure communication stage with session key K . During this stage, they generate a resumption secret Z , leveraging SKG. Instead of performing full authentication in subsequent sessions, the secret can be used as a parameter to quickly “resume” sessions in 0-RTT.

C. Resumption protocol

This Section presents a novel physical layer resumption protocol that allows A to send encrypted data in 0-RTT. During the secure communication stage of the authentication protocol in Fig. 10, B sends to A a look-up identifier. Then, both derive a resumption secret Z that is a function of the look-up identifier and the session parameters. The usage of a resumption secret for authentication helps avoid man-in-the-middle attacks in the scenario assumed here. Given the above, the resumption protocol follows the steps:

- 1) As before, in order to establish the link both devices perform pilot exchange. A and B obtain channel observations and generate sequences Y_A and Y_B , respectively. Furthermore, A measures the RSSI. Note that, Z and Y_A, Y_B have the same length.
- 2) Following the above, A performs the proximity detection mechanism to verify whether Bob is at the expected location. If the verification fails, she aborts the connection. If the verification succeeds she generates a fresh random nonce N_1 and reads the resumption secret Z to generate $Y^* = Z \oplus Y_A$. Then, using her Slepian Wolf decoder she calculates the new syndrome S^* , that corresponds to Y^* , and generates the session key as $K^* = \text{Hash}(Y^*)$. She also calculates the one-time alias ID that will be used for subsequent session as: $A_{\text{ID},i+1} = \text{Hash}(A||Y_A)$. A breaks her key into two parts $K^* = (K_1^*, K_2^*)$ and uses the first part to encrypt the early 0-RTT data M as $\text{Es}(K_1^*, M) = C$. The second part she uses to sign the cipher text $\text{Sign}(K_2^*, C) = T$. Finally, she sends $(S^*||A_{\text{ID},i}||N_1||C||T)$. Note that the key K^* can only be

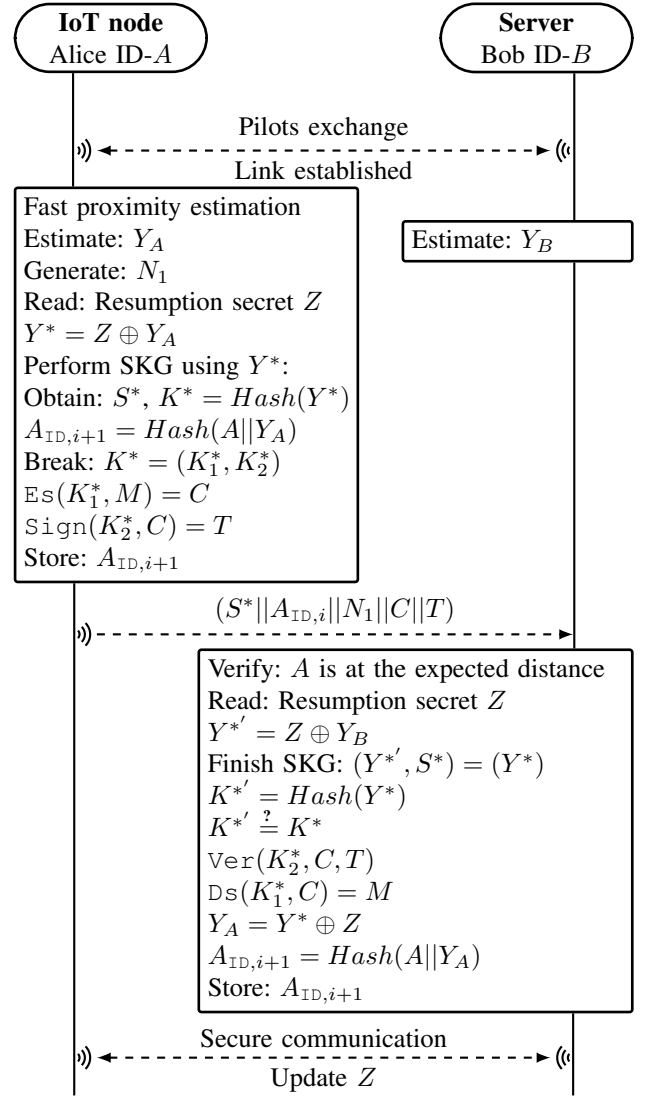


Fig. 11: Resumption protocol

obtained if both the physical layer generated key and the resumption key are valid and this method can be shown to be forward secure [51].

- 3) Upon receiving that, B reads the resumption secret Z and obtains $Y^{*'} = Z \oplus Y_B$. Using that and the received syndrome S^* , B obtains $K^* = \text{Hash}(Y^*)$. He uses the condition $K^{*'} \stackrel{?}{=} K^*$ to verify the authenticity of A and the integrity of the message. If the above succeeds he calculates $Y_A = Y^* \oplus Z$ and stores $A_{\text{ID},i+1} = \text{Hash}(A||Y_A)$.
- 4) After the resumption process finishes the two devices enter the secure communication stage using K^* as a session key. During the secure communication stage, they use the channel and session properties to generate new shared resumption secrets that can be used in subsequent resumptions.

VI. SECURITY ANALYSIS

In this Section, we analyze the security of the proposed multi-factor authentication protocol illustrated in Fig. 10. For

the purpose of our security proofs we consider a Dolev-Yao [52] type of adversary, who has control over the wireless channel between A and B . Furthermore: 1) the adversary can send any type of messages and queries using its knowledge gained through observation; 2) all functions and operations performed by the legitimate users during the execution of the protocol are public except from $P_A(\cdot)$ and the entire enrollment phase; and, 3) the adversary can launch denial of service (DoS) attacks and block parts of the protocol in order to de-synchronize the connection between A and B . In terms of the SKG, for simplicity, in this work we assume a rich Rayleigh multipath environment where the adversary is more than a few wavelengths away from each of the legitimate parties and the SKG rates are given as in Section III.

A. Mutual authentication

The proposed protocol uses a set of factors to achieve mutual authentication. It uses a fast proximity estimation as a first factor of authentication. This verifies whether the server is at the expected distance. Next, A authenticates B by verifying whether the correct key is used for creating C_B and T_B . On the other hand, B authenticates A by first confirming the validity of the received one-time alias ID $A_{ID,i}$ and second by verifying whether she produced a valid response to Ch_i . The second condition is confirmed only if A uses the correct key to generate the pair C_A, T_A .

B. Untraceability and anonymity

During the execution of the authentication protocol, A must possess a valid one-time alias ID A_{ID} for each session. The one-time alias identity cannot be used twice and there is no direct relationship between subsequent IDs. Thus, no one except B would know the origin of the message. Furthermore, in case of de-synchronization the device can use the set of emergency IDs $\mathcal{A}_{ID,emerg}$. After using an emergency ID it has to be deleted from A 's and B 's memory. This approach provides privacy against eavesdroppers and ensures user's anonymity and identity untraceability properties.

C. Perfect forward secrecy

Assuming an attacker compromises A and obtains all stored secrets, i.e., (K_R, A_{ID}) , he cannot obtain previous keys or one-time alias IDs. First, each K_R is generated using a CRP and CRPs are randomly generated and independent. Hence, by obtaining $K_{R,i}$ an adversary cannot learn $K_{R,i-1}$. Next, one-time alias IDs are generated using a one-way hash function of unique parameters for each session; if an adversary obtains $A_{ID,i}$, he can not inverse the hash function. Furthermore, using the randomness of the wireless channel ensures that session keys are unique and independent for each session. Therefore, the proposed authentication protocol ensures the perfect forward secrecy property.

D. Protection against replay attack

If an adversary intercepts previous communication between A and B , he can replay the same messages and try to pass

the authentication process. In the protocol presented in Fig. 10 none of the parameters in the initial request are allowed to be sent twice, hence, if an attacker resends the same message to B the attack will be detected and the request will be rejected. Next, if the adversary tries to re-send C_B to A , he will be detected, since the key used to encrypt C_B is changed during every session. Similarly, if the adversary tries to re-send C_A , he will be detected and the request will be rejected because the key used to encrypt C_A is changed every session. The above shows that the proposed protocol provides resistance against replay attacks.

E. Protection against impersonation attack

A successful impersonation attack will allow the adversary to be authenticated as a legitimate user. Following from above, an adversary cannot perform a replay attack, which limits his options to perform an impersonation attack. Following from that, in order to impersonate A he must generate 1) a valid one-time alias ID, and, 2) a valid ciphertext C_A . However, due to the unclonability properties of the PUF and the fact that the connection between a device and its PUF is secure, (i.e., system on chip) the adversary cannot generate a valid ciphertext C_A , hence cannot impersonate A . Next, in order to impersonate B , the adversary must possess a valid key $K_{R,1}$ and generate a valid ciphertext C_B . To obtain the key an adversary must compromise A (an example of such a scheme vulnerable to this attack can be found in [25]). However, even if A gets compromised the attack will be detected using the proposed proximity detection approach. This shows that our multi-factor authentication protocol provides resistance against impersonation attacks.

F. Resistance to DoS attack

To ensure security against DoS and de-synchronization attacks, the authentication protocol uses unlinkable one-time alias IDs and pairs of sets with emergency parameters $(\mathcal{C}_{emerg}, \mathcal{R}_{emerg})$ and $(\mathcal{K}_{R,emerg}, \mathcal{A}_{ID,emerg})$. If an adversary manages to block a message from a legitimate party, such that it does not reach its intended receiver, the authentication process will stop and the used $A_{ID,i}$ will not be updated. To overcome that A can use one of her emergency IDs from the set $\mathcal{A}_{ID,emerg}$. B will then read the corresponding $K_{R,emerg}$ from the set $\mathcal{K}_{R,emerg}$ and use it to encrypt a message containing an emergency challenge C_{emerg} from the set \mathcal{C}_{emerg} . Next, both parties can continue the authentication process as usual and setup a new one-time alias ID. In order to prevent replay attacks all used emergency parameters must be deleted from the corresponding set. This approach provides resiliency against DoS to de-synchronization attacks.

G. Protection against cloning attacks

A successful cloning attack allows the adversary to use a captured device in order to obtain secrets stored on another device. In the proposed protocol each device possesses a unique pair (K_R, A_{ID}) . Furthermore, all devices have unique PUFs and will produce a unique response to a challenge. Hence, the adversary cannot use secrets derived from one device in order to clone another.

$$\begin{array}{c}
\frac{B \equiv \#(N_B) \wedge B \stackrel{K_{R_3,2}}{\triangleleft} R_3 \mathfrak{R} N_B}{B \equiv \#(R_3)} \wedge \frac{B \equiv A \stackrel{K_{R_3,2}}{\leftrightarrow} B \wedge B \stackrel{K_{R_3,2}}{\triangleleft} R_3}{B \equiv A \stackrel{K_{R_3,2}}{\sim} R_3} \\
\hline
\frac{B \equiv A \stackrel{K_{R_3,2}}{\leftrightarrow} B}{B \equiv A \stackrel{K_{R_3,2}}{\leftrightarrow} B} \wedge \frac{B \equiv A \equiv A^c \triangleleft \parallel R_3 \wedge B \equiv A \stackrel{K_{R_3,2}}{\sim} R_3}{B \equiv A \stackrel{K_{R_3,2}}{\leftrightarrow} B} \\
\hline
\frac{B \equiv A \equiv \{B \cup A\}^c \triangleleft \parallel R_3}{B \equiv A \equiv \{B \cup A\}^c \triangleleft \parallel R_3} \wedge \frac{B \equiv \sup(A)}{B \equiv \sup(A)} \\
\hline
\frac{B \equiv \{B \cup A\}^c \triangleleft \parallel R_3}{B \equiv \{B \cup A\}^c \triangleleft \parallel R_3} \wedge \frac{B \equiv \#(R_3)}{B \equiv \#(R_3)} \\
\hline
\frac{B \equiv \{B \cup A\}^c \triangleleft \parallel R_3}{B \equiv A \stackrel{R_3}{\leftrightarrow} B}
\end{array}
\quad (a)
\quad
\begin{array}{c}
\frac{A \equiv A \stackrel{K_{R_3,2}}{\leftrightarrow} B \wedge A \equiv B^c \triangleleft \parallel R_3 \wedge A \stackrel{K_{R_3,2}}{\sim} R_3}{A \equiv \{A \cup B\}^c \triangleleft \parallel R_3} \wedge \frac{A \equiv \#(R_3)}{A \equiv \#(R_3)} \\
\hline
\frac{A \equiv \{A \cup B\}^c \triangleleft \parallel R_3}{A \equiv A \stackrel{R_3}{\leftrightarrow} B} \\
\hline
\frac{A \equiv \{A \cup B\}^c \triangleleft \parallel R_3}{A \equiv \{A \cup B\}^c \triangleleft \parallel R_3} \wedge \frac{A \equiv \sup(A)}{A \equiv \sup(A)} \\
\hline
\frac{A \equiv \{A \cup B\}^c \triangleleft \parallel R_3}{A \equiv \{A \cup B\}^c \triangleleft \parallel R_3} \wedge \frac{A \equiv \#(R_3)}{A \equiv \#(R_3)} \\
\hline
\frac{A \equiv \{A \cup B\}^c \triangleleft \parallel R_3}{A \equiv A \stackrel{R_3}{\leftrightarrow} B}
\end{array}
\quad (b)$$

$$\begin{array}{c}
\frac{A \equiv \#(N_1) \wedge A \stackrel{K_{R_1,1}}{\triangleleft} N_B \mathfrak{R} N_1}{A \equiv \#(N_B)} \wedge \frac{A \equiv A \stackrel{K_{R_1,1}}{\leftrightarrow} B \wedge A \stackrel{K_{R_1,1}}{\triangleleft} N_B}{A \equiv B \stackrel{K_{R_1,1}}{\sim} N_B} \\
\hline
\frac{A \equiv B \equiv A \stackrel{K_{R_1,1}}{\leftrightarrow} B}{A \equiv B \equiv A \stackrel{K_{R_1,1}}{\leftrightarrow} B} \wedge \frac{A \equiv B \equiv B^c \triangleleft \parallel N_B \wedge A \equiv B \stackrel{K_{R_1,1}}{\sim} N_B}{A \equiv B \equiv A \stackrel{K_{R_1,1}}{\leftrightarrow} B} \\
\hline
\frac{A \equiv B \equiv \{A \cup B\}^c \triangleleft \parallel N_B}{A \equiv B \equiv \{A \cup B\}^c \triangleleft \parallel N_B} \wedge \frac{A \equiv \sup(B)}{A \equiv \sup(B)} \\
\hline
\frac{A \equiv \{A \cup B\}^c \triangleleft \parallel N_B}{A \equiv \{A \cup B\}^c \triangleleft \parallel N_B} \wedge \frac{A \equiv \#(N_B)}{A \equiv \#(N_B)} \\
\hline
\frac{A \equiv \{A \cup B\}^c \triangleleft \parallel N_B}{A \equiv A \stackrel{N_B}{\leftrightarrow} B}
\end{array}
\quad (c)
\quad
\begin{array}{c}
\frac{B \equiv A \stackrel{K_{R_1,1}}{\leftrightarrow} B \wedge B \equiv A^c \triangleleft \parallel N_B \wedge B \stackrel{K_{R_1,1}}{\sim} N_B}{B \equiv \{B \cup A\}^c \triangleleft \parallel N_B} \wedge \frac{B \equiv \#(N_B)}{B \equiv \#(N_B)} \\
\hline
\frac{B \equiv \{B \cup A\}^c \triangleleft \parallel N_B}{B \equiv A \stackrel{N_B}{\leftrightarrow} B} \\
\hline
\frac{B \equiv \{B \cup A\}^c \triangleleft \parallel N_B}{B \equiv \{B \cup A\}^c \triangleleft \parallel N_B} \wedge \frac{B \equiv \sup(B)}{B \equiv \sup(B)} \\
\hline
\frac{B \equiv \{B \cup A\}^c \triangleleft \parallel N_B}{B \equiv \{B \cup A\}^c \triangleleft \parallel N_B} \wedge \frac{B \equiv \#(N_B)}{B \equiv \#(N_B)} \\
\hline
\frac{B \equiv \{B \cup A\}^c \triangleleft \parallel N_B}{B \equiv A \stackrel{N_B}{\leftrightarrow} B}
\end{array}
\quad (d)$$

Fig. 12: Secrecy proofs: (a) B believes R_3 is a good shared secret between A and B ; (b) A believes R_3 is a good shared secret between A and B ; (c) A believes N_B is a good shared secret between A and B ; (d) B believes N_B is a good shared secret between A and B .

H. Protection against physical attacks

Successful physical attacks could be performed by physical tampering of the IoT device in order to change its behavior. However, by changing its behavior, the PUF will not produce the desired response and therefore B will detect the attack. Therefore, the proposed protocol is resistant against physical attacks.

I. Secrecy proofs using BAN and MB logic

The secrecy evaluation of security protocols ensures that an adversary cannot obtain or alter secret parameters. In this regards, the BAN logic [12] is a widely used secrecy verification tool. However, some weaknesses were identified by the authors of [53]. They extended and improved the BAN logic to a more reliable version, namely MB logic, which is used in this paper. Formal proofs are deduced using a set of initial beliefs and rules and are based upon the message exchange within the protocol. The initial steps of MB logic are idealization of the protocol and identification of the initial beliefs. The protocol message idealization is used to interpret the implicit context-dependent information into explicit protocol specification. Based on the set of rules defined in [53], the protocol in Fig. 10 is idealised as:

- 1) $A \rightarrow B : A, N_1$
- 2) $B \rightarrow A : \{N_B \mathfrak{R} N_1\}_{K_{R_1,1}}$
- 3) $A \rightarrow B : \{R_3 | R_4 \mathfrak{R} N_A \mathfrak{R} N_B\}_{K_{R_3,2}}$

where \mathfrak{R} gives the relation of the parameters, as defined in [53]. Next, denoting principal as A, B , messages and keys as M, K , respectively and formulas as X , the main properties of MB logic are: $A \equiv X$ denotes A believes X is true; $A \stackrel{K}{\triangleleft} M$ denotes A sees M using key K , if M is not encrypted we have

TABLE II: Inference rules adopted from MB logic

Notation	Description
$\frac{A \equiv A \stackrel{K}{\leftrightarrow} B \wedge A \stackrel{K}{\triangleleft} M}{A \equiv B \stackrel{K}{\sim} M}$	Authentication rule
$\frac{A \equiv A \stackrel{K}{\leftrightarrow} B \wedge B^C \triangleleft \parallel M \wedge A \stackrel{K}{\sim} M}{A \equiv (A \cup B)^C \triangleleft \parallel M}$	Confidentiality rule
$\frac{A \equiv \#(M) \wedge A \triangleleft N \mathfrak{R} M}{A \equiv \#(N)}$	Fresh rule
$\frac{A \equiv \{A, B\}^C \triangleleft \parallel K \wedge A \equiv \#(K)}{A \equiv A \stackrel{K}{\leftrightarrow} B}$	Good-key rule
$\frac{A \equiv \#(N) \wedge A \equiv B \stackrel{K}{\sim} N}{A \equiv B \equiv A \stackrel{K}{\leftrightarrow} B}$	Nonce verification rule
$\frac{A \equiv B \equiv X \wedge A \equiv \sup(B)}{A \equiv X}$	Super-principal rule
$\frac{A \equiv X \wedge A \equiv Y}{A \equiv (X \wedge Y)}$	Belief axiom 1
$\frac{A \equiv X \wedge A \equiv X/Y}{A \equiv Y}$	Belief axiom 2

$A \triangleleft M$; $A \stackrel{K}{\sim} M$ denotes A encrypts M using key K ; $\#(M)$ denotes M is of type fresh; $A \stackrel{K}{\leftrightarrow} B$ denotes K is a good shared key between A and B ; $A \triangleleft \parallel M$ denotes M is not available to A ; $\sup(B)$ denotes B is a super-principal. Following that, the inference rules defined in [53] and used in this paper are given in Table II (Note, $\{\cdot\}^C$ denotes complement). Given the above we define the initial beliefs as follows:

$$\begin{array}{c}
\frac{A \equiv A \overset{K_{R,1}}{\leftrightarrow} B \wedge A \overset{K_{R,1}}{\triangleleft} N_B}{A \equiv B \overset{K_{R,1}}{\sim} N_B} \\
\text{(a)}
\end{array}
\quad
\begin{array}{c}
\frac{A \equiv A \overset{K_{R',2}}{\leftrightarrow} B \wedge B \overset{K_{R',2}}{\triangleleft} N_A}{B \equiv A \overset{K_{R',2}}{\sim} N_A} \\
\text{(b)}
\end{array}$$

Fig. 13: Proof of authentication (a) B to A ; (b) A to B .

$$\begin{array}{l}
\text{A1 } A \equiv A \overset{K_{R,1}}{\leftrightarrow} B \text{ and } B \equiv A \overset{K_{R,1}}{\leftrightarrow} B \\
\text{A2 } A \equiv A \overset{K'_{R,2}}{\leftrightarrow} B \text{ and } B \equiv A \overset{K'_{R,2}}{\leftrightarrow} B \\
\text{A3 } B \equiv A \equiv A^C \triangleleft ||R_3|R_4\mathfrak{R}N_A\mathfrak{R}N_B \\
\text{A4 } B \equiv \text{sup}(A) \\
\text{A5 } B \overset{K'_{R,2}}{\triangleleft} R_3|R_4\mathfrak{R}N_A\mathfrak{R}N_B \\
\text{A6 } A \equiv B^C \triangleleft ||R_3|R_4\mathfrak{R}N_A\mathfrak{R}N_B \\
\text{A7 } A \overset{K_{R,2}}{\sim} R_3|R_4\mathfrak{R}N_A\mathfrak{R}N_B \\
\text{A8 } A \equiv \#(N_1), A \equiv \#(N_A), A \equiv \#(R_3), A \equiv \#(R_4) \\
\text{A9 } A \overset{K_{R,1}}{\triangleleft} N_B\mathfrak{R}N_1 \\
\text{A10 } A \equiv B \equiv B^C \triangleleft ||N_B \text{ and } B \equiv \#(N_B) \\
\text{A11 } A \equiv \text{sup}(B) \\
\text{A12 } B \equiv A^C \triangleleft ||N_B\mathfrak{R}N_1 \\
\text{A13 } B \overset{K_{R,1}}{\sim} N_B\mathfrak{R}N_1
\end{array}$$

The authentication property of the current run of the protocol can be verified using the authentication rule as shown on Fig. 13. The authentication of B to A can be achieved by the fact $A \equiv B \overset{K_{R,1}}{\sim} N_B$, i.e., A believes that B sent N_B using $K_{R,1}$ to encrypt the message. As seen in Fig. 13, two facts imply authentication 1) $A \equiv A \overset{K_{R,1}}{\leftrightarrow} B$ meaning A believes that $K_{R,1}$ is a good shared secret between A and B ; 2) $A \overset{K_{R,1}}{\triangleleft} N_B$, i.e., A used $K_{R,1}$ as a decryption key to see N_B . Following from the fact that the enrollment stage is performed on a secure channel both of these statements are part of the initial beliefs of the protocol, hence, the authentication of B to A is directly established as shown on Fig. 13 a). The authentication of A to B is identical following from Fig. 13 b). Next, we prove the secrecy of parameters R_3 (the proofs for secrecy of N_A and R_4 are identical) which could be used as initial belief for the next run of the protocol. First, by combining the confidentiality rule and two axioms from Table II the following rule is derived:

$$\frac{A \equiv B \overset{K}{\sim} M \wedge A \equiv B \equiv A \overset{K}{\leftrightarrow} B \wedge A \equiv B \equiv B^C \triangleleft ||M}{A \equiv B \equiv \{A \cup B\}^C \triangleleft ||M}. \quad (7)$$

Given that, the security proofs on Fig. 12 (a) and (b) show that both parties A and B agree that R_3 is a good shared secret (similarly, one can show the property holds for R_4). Given that and using the fuzzy extractor properties [31] it can be concluded that $K_{R,3}$ and $K_{R,4}$ are good shared keys between A and B . Next, Fig. 12 (c) and (d) illustrates that A and B agree that N_B is a good shared secret. As a consequence of the above and by using the properties of privacy amplification [54] we can conclude that $A_{ID,2}$ is also a good shared secret.

J. Session key agreement

It is a common practice in literature to use nonces as part of the session key generation process [24]–[26]. However, note that even if N_A and N_B are good shared secrets between A and B the low entropy of pseudo-random number generator (PRNG) modules may provoke a set of attacks, such as side-channel and prediction attacks [55], and lead to information leakage. Furthermore, it has been shown that true-random number generators (TRNGs) can greatly increase the time complexity in a resource limited systems making the generation time infeasible [56]. Therefore, we limit the role of the nonces in the proposed scheme to only a source of freshness. On the other hand, the randomness already present in the wireless channel allows for a secure and lightweight key generation process through the SKG procedure, as illustrated in Section III. Finally, we note that if the session key somehow gets compromised, the authentication process remains secure as the adversary cannot obtain the PUF response using the session key.

K. Security verification using the Tamarin-prover

The security properties of the authentication protocol given in Section V were verified using the formal verification tool, Tamarin-prover [13]. Tamarin was used to prove: secrecy, aliveness, weak agreement, non-injective agreement, injective agreement, untraceability and anonymity. The model of our authentication protocol in Tamarin syntax is provided in the supplementary material to this paper, due to space limitations.

VII. CONCLUSIONS

In this work we introduced a fast, multi-factor mutual authentication protocol for IoT systems, leveraging SKG from fading coefficients, proximity estimation using Kalman filters and PUFs. To demonstrate the SKG performance in delay constrained applications we provided a numerical comparison of three families of channel SW codes in the short and medium blocklength regimes. Next, we conducted a set of experiments to demonstrate the applicability of our proposed fast proximity detection in BLE networks, that leverages mobility of an IoT node. Finally, we validated the properties of the proposed authentication protocol through a detailed security analysis, using BAN and MB logic as well as the Tamarin-prover. Our analysis proves the potential of the proposed protocol as a lightweight, multi-factor alternative to the currently used computationally intensive authentication schemes, with a particular interest in IoT networks of constrained devices and wireless sensor networks.

REFERENCES

- [1] I. Stellios, P. Kotzanikolaou, M. Psarakis, C. Alcaraz, and J. Lopez, "A survey of IoT-enabled cyberattacks: Assessing attack paths to critical infrastructures and services," *IEEE Commun. Surveys Tuts.*, vol. 20, no. 4, pp. 3453–3495, 2018.
- [2] D. Karatzas, A. Chorti, N. M. White, and C. J. Harris, "Teaching old sensors new tricks: Archetypes of intelligence," *IEEE Sensors J.*, vol. 7, no. 5, pp. 868–881, May 2007.
- [3] A. Teniou and B. A. Bensaber, "Efficient and dynamic elliptic curve qu-vanstone implicit certificates distribution scheme for vehicular cloud networks," *Security and Privacy*, Jan. 2018.

- [4] “3GPP TR 33.825 V0.3.0, Study on the Security for 5G URLLC (Release 16),” 3rd Generation Partnership Project; Technical Specification Group Services and System Aspects.
- [5] A. Chorti and H. V. Poor, “Achievable secrecy rates in physical layer secure systems with a helping interferer,” in *2012 Int. Conf. Computing, Netw. Commun. (ICNC)*, Jan 2012, pp. 18–22.
- [6] A. Chorti, C. Hollanti, J. Belfiore, and H. V. Poor, “Physical layer security: A paradigm shift in data confidentiality,” *Lecture Notes Electr. Eng.*, vol. 358, Jan 2016.
- [7] M. Mitev, A. Chorti, M. Reed, L. Musavian, “Authenticated secret key generation in delay-constrained wireless systems,” *EURASIP JWCN*, no. 122, June 2020.
- [8] M. Mitev, A. Chorti, and M. Reed, “Subcarrier scheduling for joint data transfer and key generation schemes in multicarrier systems,” in *IEEE Global Commun. Conf. (GLOBECOM)*, Dec 2019, pp. 1–6.
- [9] M. Mitev, A. Chorti, E. V. Belmega, and M. Reed, “Man-in-the-middle and denial of service attacks in wireless secret key generation,” in *IEEE Global Commun. Conf. (GLOBECOM)*, Dec 2019, pp. 1–6.
- [10] B. Gassend, D. Clarke, M. van Dijk, and S. Devadas, “Silicon physical random functions,” in *Proc. of the 9th ACM Conference on Computer and Communications Security*, 2002, pp. 148–160.
- [11] C. Herder, M. Yu, F. Koushanfar, and S. Devadas, “Physical unclonable functions and applications: A tutorial,” *Proc. IEEE*, vol. 102, 2014.
- [12] M. Burrows, M. Abadi, and R. Needham, “A logic of authentication,” *ACM Trans. Comput. Syst.*, vol. 8, no. 1, pp. 18–36, Feb. 1990.
- [13] S. Meier, B. Schmidt, C. Cremers, and D. Basin, “The tamarin prover for the symbolic analysis of security protocols,” in *Proc. of the 25th Int. Conf. on Comp. Aided Ver.*, vol. 8044, 2013, pp. 696–701.
- [14] J. Zhang, T. Q. Duong, A. Marshall, and R. Woods, “Key generation from wireless channels: A review,” *IEEE Access*, vol. 4, 2016.
- [15] B. Chen, T. Ignatenko, F. M. J. Willems, R. Maes, E. van der Sluis, and G. Selimis, “A robust SRAM-PUF key generation scheme based on polar codes,” in *Proc. IEEE Global Commun. Conf.*, 2017, pp. 1–6.
- [16] R. Maes, A. Van Herwege, and I. Verbauwhede, “PUFKY: A fully functional PUF-based cryptographic key generator,” in *Cryptographic Hardware and Embedded Systems – CHES*, 2012, pp. 302–319.
- [17] R. A. Chou, M. R. Bloch, and E. Abbe, “Polar coding for secret-key generation,” *IEEE Trans. Inf. Theory*, vol. 61, no. 11, 2015.
- [18] H. Hentilä, Y. Y. Shkel, V. Koivunen, and H. V. Poor, “On polar coding for finite blocklength secret key generation over wireless channels,” in *Proc. IEEE Int. Conf. Acoustics, Speech and Signal Process. (ICASSP)*, 2020, pp. 5265–5269.
- [19] M. Shirvanimoghaddam, M. S. Mohammadi, R. Abbas, A. Minja, C. Yue, B. Matuz, G. Han, Z. Lin, W. Liu, Y. Li, S. Johnson, and B. Vucetic, “Short block-length codes for ultra-reliable low latency communications,” *IEEE Commun. Mag.*, vol. 57, no. 2, 2019.
- [20] G. Liva, L. Gaudio, T. Ninacs, and T. Jerkovits, “Code design for short blocks: A survey,” *arXiv preprint arXiv:1610.00873*, 2016.
- [21] H. Wang, Y. Wen, Y. Lu, D. Zhao, and C. Ji, “Secure localization algorithms in wireless sensor networks: A review,” in *Advances in Computer Communication and Computational Sciences*, 2019.
- [22] X. Chen, K. Makki, K. Yen, and N. Pissinou, “Sensor network security: A survey,” *IEEE Commun. Surveys Tuts.*, vol. 11, no. 2, pp. 52–73, 2009.
- [23] I. Domuta and T. P. Palade, “On-line estimation of base station location,” *IEEE Wireless Commun. Lett.*, vol. 9, no. 3, pp. 331–335, 2020.
- [24] M. N. Aman, M. H. Basheer, and B. Sikdar, “Two-factor authentication for IoT with location information,” *IEEE Internet Things J.*, vol. 6, no. 2, pp. 3335–3351, April 2019.
- [25] P. Gope and B. Sikdar, “Lightweight and privacy-preserving two-factor authentication scheme for IoT devices,” *IEEE Internet Things J.*, vol. 6, no. 1, pp. 580–589, 2019.
- [26] P. Gope and B. Sikdar, “Privacy-aware authenticated key agreement scheme for secure smart grid communication,” *IEEE Trans. Smart Grid*, vol. 10, no. 4, pp. 3953–3962, 2019.
- [27] J. Delvaux, R. Peeters, D. Gu, and I. Verbauwhede, “A survey on lightweight entity authentication with strong PUFs,” *ACM Comput. Surv.*, vol. 48, no. 2, 2015.
- [28] A. Babaei and G. Schiele, “Physical unclonable functions in the internet of things: State of the art and open challenges,” in *Sensors*, 2019.
- [29] P. Gope and B. Sikdar, “Lightweight and privacy-preserving two-factor authentication scheme for IoT devices,” *IEEE Internet Things J.*, vol. 6, no. 1, pp. 580–589, 2019.
- [30] P. Gope, J. Lee, and T. Q. S. Quek, “Lightweight and practical anonymous authentication protocol for RFID systems using physically unclonable functions,” *IEEE Trans. Inf. Forensics and Security*, vol. 13, no. 11, pp. 2831–2843, 2018.
- [31] B. Fuller, L. Reyzin, and A. Smith, “When are fuzzy extractors possible?” *IEEE Trans. Inf. Theory*, vol. 66, no. 8, pp. 5282–5298, 2020.
- [32] P. Li, J. Su, and X. Wang, “ITLS: Lightweight transport layer security protocol for IoT with minimal latency and perfect forward secrecy,” *IEEE Internet Things J.*, 2020.
- [33] S. N. Premnath, S. Jana, J. Croft, P. L. Gowda, M. Clark, S. K. Kasera, N. Patwari, and S. V. Krishnamurthy, “Secret key extraction from wireless signal strength in real environments,” *IEEE Trans. Mobile Comput.*, vol. 12, no. 5, pp. 917–930, 2013.
- [34] X. Zhu, F. Xu, E. Novak, C. C. Tan, Q. Li, and G. Chen, “Using wireless link dynamics to extract a secret key in vehicular scenarios,” *IEEE Trans. Mobile Comput.*, vol. 16, no. 7, pp. 2065–2078, 2017.
- [35] W. Xu, S. Jha, and W. Hu, “LoRa-Key: Secure key generation system for LoRa-based network,” *IEEE Internet Things J.*, vol. 6, no. 4, pp. 6404–6416, 2019.
- [36] W. Zhou and M. Lentmaier, “Improving short-length LDPC codes with a CRC and iterative ordered statistic decoding : (invited paper),” in *53rd Annual Conf. Inf. Sciences Systems (CISS)*, 2019, pp. 1–6.
- [37] I. Tal and A. Vardy, “List decoding of polar codes,” *IEEE Trans. Inf. Theory*, vol. 61, no. 5, pp. 2213–2226, 2015.
- [38] M. P. C. Fossorier and Shu Lin, “Soft-decision decoding of linear block codes based on ordered statistics,” *IEEE Trans. Inf. Theory*, vol. 41, no. 5, pp. 1379–1396, 1995.
- [39] H. Tyagi and S. Watanabe, “Converses for secret key agreement and secure computing,” *IEEE Trans. Inf. Theory*, vol. 61, no. 9, 2015.
- [40] T. J. Richardson, M. A. Shokrollahi, and R. L. Urbanke, “Design of capacity-approaching irregular low-density parity-check codes,” *IEEE Trans. Inf. Theory*, vol. 47, no. 2, pp. 619–637, 2001.
- [41] Y. Wu and C. N. Hadjicostis, “Soft-decision decoding using ordered recodings on the most reliable basis,” *IEEE Trans. Inf. Theory*, vol. 53, no. 2, pp. 829–836, 2007.
- [42] E. Arikan, “Channel polarization: A method for constructing capacity-achieving codes for symmetric binary-input memoryless channels,” *IEEE Trans. Inf. Theory*, vol. 55, no. 7, pp. 3051–3073, 2009.
- [43] E. Arikan, “Source polarization,” in *IEEE Int. Symp. Inf. Theory*, 2010.
- [44] M. Shakiba-Herfeh, A. K. Tanc, and T. M. Duman, “LDPC code design for fading interference channels,” *IEEE Trans. Veh. Technol.*, vol. 68, no. 3, pp. 2374–2385, 2019.
- [45] S. Balakrishna and M. Thirumaran, “Semantic interoperable traffic management framework for IoT smart city applications,” *EAI Endorsed Transactions on Internet of Things*, vol. 4, p. 155482, 09 2018.
- [46] J. B. Andersen, T. S. Rappaport, and S. Yoshida, “Propagation measurements and models for wireless communications channels,” *IEEE Commun. Mag.*, vol. 33, no. 1, pp. 42–49, 1995.
- [47] H. A. Nguyen, H. Guo, and K. Low, “Real-time estimation of sensor node’s position using particle swarm optimization with log-barrier constraint,” *IEEE Trans. Instrum. Measurement*, vol. 60, 2011.
- [48] T. Rappaport, *Wireless Communications: Principles and Practice*, 2nd ed. USA: Prentice Hall PTR, 2001.
- [49] P. Spachos and K. N. Plataniotis, “BLE beacons for indoor positioning at an interactive IoT-based smart museum,” *IEEE Systems J.*, vol. 14, no. 3, pp. 3483–3493, 2020.
- [50] G. Welch and G. Bishop, “An introduction to the Kalman filter,” University of North Carolina at Chapel Hill, USA, Tech. Rep., 1995.
- [51] N. Aviram, K. Gellert, and T. Jager, “Session resumption protocols and efficient forward security for TLS 1.3 0-RTT,” Cryptology ePrint Archive, Report 2019/228, 2019.
- [52] D. Dolev and A. Yao, “On the security of public key protocols,” *IEEE Trans. Inf. Theory*, vol. 29, no. 2, pp. 198–208, 1983.
- [53] W. Mao and C. Boyd, “Towards formal analysis of security protocols,” in *Proc. Computer Security Foundations Workshop VI*, 1993, pp. 147–158.
- [54] C. H. Bennett, G. Brassard, C. Crepeau, and U. M. Maurer, “Generalized privacy amplification,” *IEEE Trans. Inf. Theory*, vol. 41, no. 6, 1995.
- [55] T. Miki, N. Miura, H. Sonoda, K. Mizuta, and M. Nagata, “A random interrupt dithering SAR technique for secure ADC against reference-charge side-channel attack,” *IEEE Trans. Circuits Syst., II, Exp. Briefs*, vol. 67, no. 1, pp. 14–18, 2020.
- [56] C. Huth, D. Becker, J. G. Merchan, P. Duplys, and T. Güneysu, “Securing systems with indispensable entropy: LWE-based lossless computational fuzzy extractor for the internet of things,” *IEEE Access*, vol. 5, pp. 11 909–11 926, 2017.